

Radiative Decoupling as a Boundary Condition: A Geometric Normalization from Stellar Photospheres to the Cosmic Horizon

NADAV BASHAN¹

¹*Independent Researcher*

ABSTRACT

Astrophysical measurements are anchored in 2D radiative decoupling surfaces, the loci where photons escape and propagate freely, providing direct operational access to physical systems.

In this Letter, we formalize radiative decoupling as a geometric boundary condition. By coupling radiative observables with Newtonian surface gravity, we define a dimensionless boundary relation. Under standard macroscopic closures, mass and bulk gravity cancel, reducing the relation to an exact mass independent geometric phase space capacity, $\pi^3/15 \simeq 2.0671$.

Observationally, using independently determined solar inputs and a kinematic sample of 190 detached eclipsing binaries, we find stellar photospheres to cluster below this theoretical upper bound.

Projecting this 2D surface normalization to the cosmic horizon yields a master equation, $\Lambda R_H^2 = \pi^3/15$. This identity yields a geometric derivation for the dark energy fraction, $\Omega_\Lambda = \pi^3/45 \simeq 0.6890$, natively without parameter tuning.

Encoding this constraint into a mini superspace action recovers the Friedmann expansion rate and the Bekenstein Hawking entropy scaling ($N = A_H/l_P^2$). The canonical 10^{120} vacuum discrepancy is reframed as the dimensional area scaling ratio bridging the macroscopic horizon and the microscopic Planck scale.

Finally, modeling the transition from a continuous primordial fluid to a discrete late time void network via 3D optimal sphere packing ($k = 12$) generates structural gaps and implies a kinematic metric stretch, $H_0^{\text{local}} = H_0^{\text{CMB}}(13/12) \simeq 73.01 \text{ km s}^{-1} \text{ Mpc}^{-1}$.

Keywords: Cosmological parameters (339), Cosmological matter density (343), Dark energy (351), Hubble constant (758), Stellar photospheres (1620), Topology (114)

1. INTRODUCTION: THE MACROSCOPIC BOUNDARY PRINCIPLE

Astrophysical inference is anchored in loci where radiation becomes observationally accessible. Operationally, a physical system becomes measurable only at surfaces where photons decouple from matter and propagate freely. The stellar photosphere represents the local, accessible archetype of such a boundary; the cosmic microwave background (CMB) and the late-time Hubble horizon operate as its global analogs.

Standard theoretical frameworks have historically treated such boundaries merely as observational transition zones, constructing cosmology predominantly around the internal bulk fluid dynamics of the Fried-

mann equations. Consequently, anomalous observations like accelerated cosmic expansion are routinely addressed by inventing unobservable, fine-tuned microscopic bulk fluids (e.g., dark energy). We identify the attempt to force overarching macroscopic constraints into microscopic state dynamics as a profound category error. Cosmic expansion is structurally a phenomenon of the geometric envelope, not of microscopic particle interaction.

In this paper, we formalize the Macroscopic Boundary Principle: the operational principle that stable macroscopic systems are governed strictly by the geometry of their decoupling surfaces. By formulating a dimensionless relation that can be evaluated across vastly different scales, we examine whether a single geometric capacity constrains photon decoupling from stellar surfaces to the observable limits of the universe. The primary result of this paper is the derivation and empirical evaluation

of a single boundary equation linking cosmological constraints to geometric capacities. The methodology follows a strict dimensional hierarchy: defining the local boundary relation, testing it empirically against stellar benchmarks, projecting it macroscopically to the cosmic horizon, formally verifying its dynamic and thermodynamic consistency, and finally interpreting its kinematic implications.

2. THE DECOUPLING BOUNDARY RELATION

We define a dimensionless boundary relation directly from standard macroscopic observables: luminosity L , mass M , radius R , effective temperature T_{eff} , and Newtonian surface gravity g . This relation couples the radiative output with the gravitational retention strictly at the boundary interface:

$$X \equiv \left(\frac{L G M}{g R^4 T_{\text{eff}}^4} \right) \left(\frac{\hbar^3 c^2}{k_B^4} \right). \quad (1)$$

The inclusion of constants removes all physical dimensions, rendering the evaluation a pure number. Substituting the standard macroscopic Stefan–Boltzmann relation ($L = 4\pi R^2 \sigma T_{\text{eff}}^4$) and Newtonian gravity ($g = GM/R^2$) into Equation 1 causes the mass (M) and the gravitational constant (G) to cancel identically. Under these substitutions, Equation 1 reduces to $X = 4\pi\sigma(\hbar^3 c^2/k_B^4)$. Using $\sigma = \pi^2 k_B^4/(60\hbar^3 c^2)$ (derived from the integration of the Planck spectrum), the relation converges to a constant phase-space coefficient:

$$X \rightarrow \frac{\pi^3}{15} \simeq 2.0671. \quad (2)$$

While this substitution yields an exact algebraic identity, such perfect cancellations in physics often reveal fundamental structural imperatives. Analogous to the exact cancellation of inertial and gravitational mass in the classical equations of free-fall – which ultimately motivated the Equivalence Principle – the strict mathematical disappearance of mass and bulk gravity at the photosphere (Eddington 1926; Schwarzschild 1906) reflects a structural decoupling under the macroscopic closures adopted here: the evaluated boundary capacity depends only on boundary observables once the standard relations are substituted, with the interior entering only through those closures. The capacity of the decoupling surface is therefore a pure geometric invariant (see Figure 1).

Equation 2 mathematically defines a strict upper limit corresponding to a perfectly sharp decoupling surface. Real stellar photospheres, however, are physically extended, bounded by finite optical depth and atmospheric

structure. Therefore, empirical evaluations are structurally expected to lie slightly below $\pi^3/15$, approaching this maximum only in the limit of an infinitely thin, ideal boundary.

3. EMPIRICAL EVALUATION: STELLAR PHOTOSPHERES

3.1. The Independent Solar Benchmark

To verify that this geometric normalization is physically realized and not merely an artifact of circular cataloging, it must be evaluated using parameters measured strictly independently of thermal radiation models. The Sun serves as the definitive test case. Utilizing independently determined solar inputs – dynamical mass (1.9884×10^{30} kg), geometric radius (6.957×10^8 m), radiometric luminosity (3.828×10^{26} W), and spectroscopic temperature (5777 K) – yields a solar evaluation of 2.0599. The minor deviation from the strict theoretical limit ($\pi^3/15 \simeq 2.0671$) reflects the finite atmospheric extension of physical stars compared to an idealized, sharp 2D geometric boundary.

3.2. DEB Ensemble Statistics

This geometric boundary constraint is further tested against the compilation of 190 detached eclipsing-binary (DEB) components (Torres et al. 2010). In these systems, stellar mass and radius are derived kinematically and geometrically from orbital radial velocities and eclipse timing, independent of effective temperature. Evaluated component-by-component, the ensemble exhibits an empirical mean of 2.0600 with a standard deviation of 0.0027. Furthermore, plotting the absolute evaluated values against stellar mass reveals no systematic trend across roughly two decades in mass ($0.2\text{--}30 M_\odot$). This horizontal clustering observationally verifies the mass-independence predicted by the boundary cancellation (see Figure 2). Because Equation 1 contains steep inverse powers (R^{-4} , T_{eff}^{-4}), standard first-order error propagation yields explicit coefficients of 16 for the fractional uncertainties of radius and temperature. The tightly bound empirical dispersion (0.0027) is accounted for by propagated observational noise.

4. COSMOLOGICAL PROJECTION AND THE DARK SECTOR

4.1. Horizon Capacity and Dark Energy (Ω_Λ)

If $\pi^3/15$ is a scale-independent boundary condition, it should natively constrain the ultimate macroscopic decoupling surface: the cosmic horizon. The Hubble horizon area is $A_H = 4\pi(c/H_0)^2 \equiv 4\pi R_H^2$. Using $\rho_\Lambda = \Omega_\Lambda \rho_c$ with $\rho_\Lambda = \Lambda c^2/(8\pi G)$ and $\rho_c = 3H_0^2/(8\pi G)$, one obtains $\Lambda = (3H_0^2/c^2)\Omega_\Lambda = (3/R_H^2)\Omega_\Lambda$. We consider the

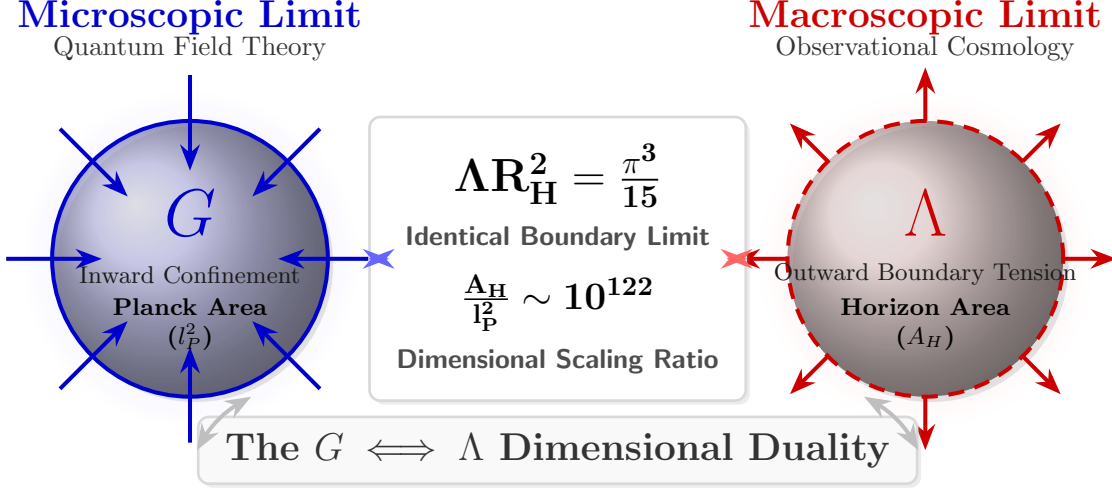


Figure 1. The $G \leftrightarrow \Lambda$ dimensional duality. Quantum field theory (left) computes the capacity of a single microscopic Planck area governed by inward Newtonian gravity (G). Observational cosmology (right) measures the integrated macroscopic horizon governed by outward boundary tension (Λ). The commonly quoted $\sim 10^{120}$ refers to an energy-density ratio, whereas $A_H/l_P^2 \sim 10^{122}$ is a discrete area-counting ratio; the distinction is inherently dimensional. The apparent discrepancy follows from mapping the macroscopic boundary to the microscopic Planck scale. Thus, G and Λ are mathematically unified as dual dimensional mappings of the same boundary normalization.

dimensionless combination ΛA_H as the horizon-capacity measure, yielding:

$$\Lambda A_H = \left(\frac{3}{R_H^2} \Omega_\Lambda \right) (4\pi R_H^2) = 12\pi \Omega_\Lambda. \quad (3)$$

Accounting for the observer-centered horizon geometry – where observers reside enclosed by the cosmic horizon rather than exterior to a stellar surface – equating this global horizon capacity to the full-sphere projection of the local boundary capacity ($4\pi[\pi^3/15]$) provides a strict geometric limit for the dark energy fraction:

$$12\pi \Omega_\Lambda = 4\pi \left(\frac{\pi^3}{15} \right) \Rightarrow \Omega_\Lambda = \frac{\pi^3}{45} \simeq 0.6890. \quad (4)$$

Rather than treating Ω_Λ as a free parameter put in by hand to match observations, this geometric target derives it natively, aligning explicitly with the [Planck Collaboration \(2020\)](#) empirical constraint of $\Omega_\Lambda = 0.6889 \pm 0.0056$ (see Figure 3).

Substituting Equation 4 back yields the unified master equation:

$$\boxed{\Lambda R_H^2 = \frac{\pi^3}{15}} \quad (5)$$

Defining the horizon scale here as $R_H \equiv c/H_0$, the macroscopic boundary tension scales as $\Lambda \propto H_0^2$. Since the critical density ρ_c is defined by H_0^2 , Equation 4 yields $\Omega_\Lambda = \pi^3/45$ directly.

4.2. Consistency Check: Emergent Dynamics and Information Bounds

To verify dynamical consistency without postulating ad-hoc bulk fluids, the kinematic boundary constraint $\Lambda(ca/\dot{a})^2 = \pi^3/15$ can be formalized as an effective zero-energy mini-superspace Lagrangian density $\mathcal{L} = (\pi^3/15c^2)a\dot{a}^2 + \Lambda a^3$. Evaluating the stationary action under the Hamiltonian constraint ($\mathcal{H} = 0$) natively yields the vacuum Friedmann expansion rate $H^2 = 15\Lambda c^2/\pi^3$. Substituting this rate into the standard density parameter definition algebraically recovers the observed attractor $\Omega_\Lambda = \pi^3/45$.

Furthermore, holographic frameworks restrict the maximum number of independent quantum degrees of freedom of a region to its bounding area ([Bousso 2002](#)). Assuming the macroscopic boundary tension corresponds to a discrete quantum state count N , the emergent gravitational coupling scales as $G = 4\pi^4 c^3/(15\hbar\Lambda N)$. Substituting the master boundary condition ($\Lambda R_H^2 = \pi^3/15$) analytically isolates the state count:

$$N = \frac{4\pi^4 c^3}{15\hbar G \left(\frac{\pi^3}{15R_H^2} \right)} = \frac{4\pi R_H^2 c^3}{\hbar G}. \quad (6)$$

Recognizing the macroscopic horizon spherical area $A_H = 4\pi R_H^2$ and the Planck area $l_P^2 \equiv \hbar G/c^3$, this explicitly recovers the fundamental Bekenstein–Hawking entropy scaling, $N = A_H/l_P^2$ ([Hawking 1975](#)), as an exact algebraic identity, formally establishing gravity as an emergent thermodynamic property of the boundary.

4.3. Dimensional Scaling and the Cosmological Constant Discrepancy

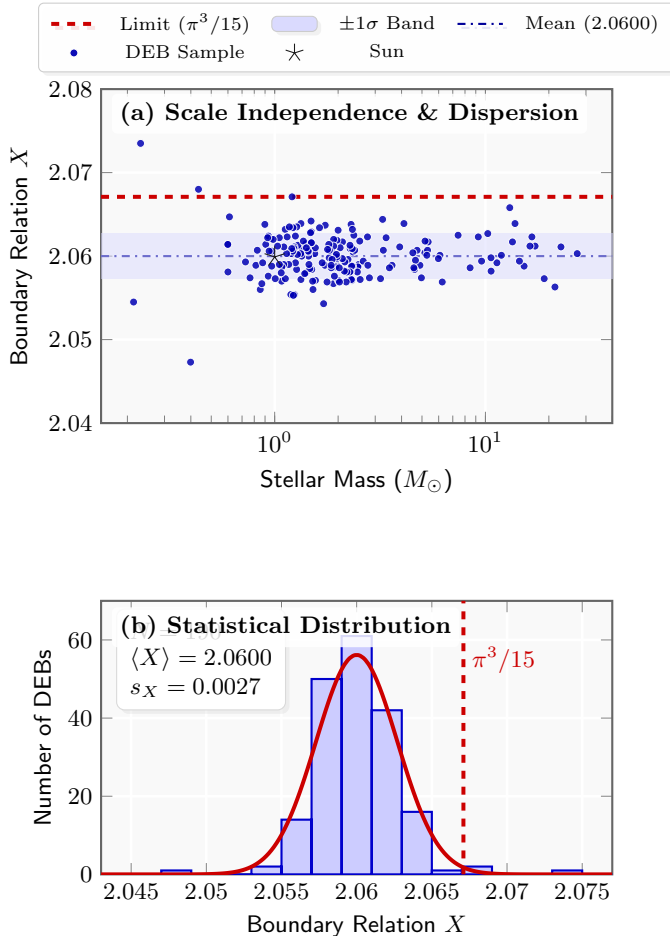


Figure 2. Dual-panel statistical analysis of the boundary relation across 190 DEB components (Torres et al. 2010). **(a)** Evaluated absolute values demonstrating scale-invariance across stellar masses. The shaded band denotes the empirical 1σ dispersion (± 0.0027). The Solar evaluation is shown as an orange star. **(b)** The raw histogram overlaid with a bin-normalized Gaussian probability density function (red curve), with variance accounted for by observational noise. The geometric limit $\pi^3/15$ (dashed red line) represents the theoretical upper bound of a mathematically sharp 2D decoupling boundary, with physical photospheres clustering slightly below it due to finite atmospheric extension.

The algebraic shift from the local boundary limit $\pi^3/15$ to the cosmological fraction $\pi^3/45$ is governed by an exact geometric factor of $1/3$. This mathematically reflects the dimensional projection required to map a strictly 2D surface-normalized capacity into a 3D Friedmann-normalized bulk parameterization, representing the area-to-volume geometric ratio $(4\pi)/(12\pi) = 1/3$.

The standard cosmological constant problem is canonically framed as a catastrophic divergence between a

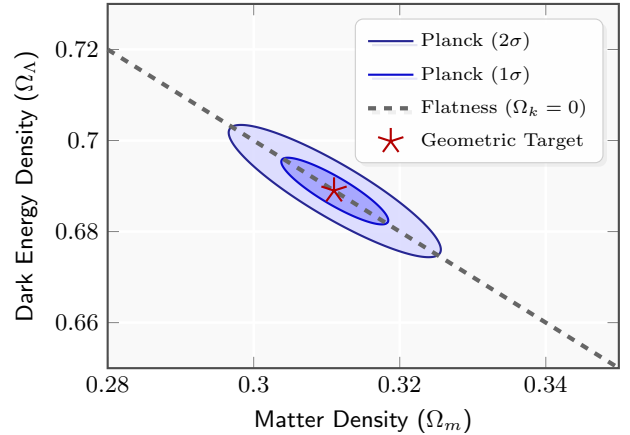


Figure 3. Cosmological constraints in the $\Omega_m - \Omega_\Lambda$ parameter space. Schematic 1σ and 2σ ellipses centered on the Planck 2020 mean are provided as a visual guide (Planck Collaboration 2020). The dashed diagonal line denotes strict spatial flatness ($\Omega_m + \Omega_\Lambda = 1$). The geometric target derived strictly from the boundary condition (orange star) lands explicitly at the empirical center of the observationally allowed domain.

quantum-field-theory (QFT) estimate of zero-point energy and the observed macroscopic value. Standard QFT integrates zero-point modes up to a Planck cutoff over a 3D bulk volume, inherently ignoring the fundamental Bekenstein bound. Conversely, holographic principles mandate that physical capacity is bounded by the discrete number of Planck-area elements (l_P^2) that can tile a 2D bounding surface. As demonstrated by the entropy scaling, this yields a dimensionless scaling for the Hubble horizon area of $N = A_H/l_P^2 \sim 10^{122}$.

The commonly quoted $\sim 10^{120}$ refers to an energy-density ratio, whereas $A_H/l_P^2 \sim 10^{122}$ is an area-counting ratio; the distinction is dimensional. Extending this established decoupling-boundary behavior to the cosmic horizon boundary physically justifies treating Λ as a macroscopic boundary tension. Within this framework, integrating a bulk Lagrangian to find a 3D volume density becomes a dimensional area-scaling artifact. The empirical fraction $\Omega_\Lambda \simeq 0.69$ and the apparent $\sim 10^{120}$ discrepancy are complementary expressions of the identical boundary constraint: the former dictates the macroscopic geometric partition of the horizon, while the latter explicitly reflects the microscopic area resolution required to saturate it.

4.4. Geometric Constraint on Ω_m

Under spatial flatness, $\Omega_{\text{tot}} = 1$, the complementary matter fraction follows directly:

$$\Omega_m = 1 - \Omega_\Lambda = 1 - \frac{\pi^3}{45} \simeq 0.3110. \quad (7)$$

In this framing, the dark-sector partition emerges given the stated geometric assumptions, without parameter tuning.

5. TOPOLOGICAL PACKING INTERPRETATION AND THE H_0 OFFSET

Early-universe inferences of H_0 are anchored to a tightly coupled radiation–baryon fluid prior to recombination; local determinations sample a late universe structured into a discrete cosmic web. If the macroscopic boundary normalization is a structural organizing principle, the mapping between these regimes may be expressed geometrically. Treating the late universe as a coarse-grained discrete structure, the transition from an effectively continuous primordial fluid to a discretized network of underdense domains carries an unavoidable geometric gap.

Packing discrete spherical domains into a 3D Euclidean volume intrinsically generates interstitial empty spaces (voids). A closed spherical membrane requires exactly 12 pentagonal defects to satisfy Euler’s polyhedron theorem (Conway & Sloane 2013). In three-dimensional Euclidean space, the local kissing number for equal spheres is exactly $k = 12$ (Conway & Sloane 2013), which serves as the strict geometric dual to the 12 Euler pentagonal defects required to mathematically close a 2D spherical membrane.

Transitioning into this maximally packed discrete network without tearing the underlying spacetime manifold structurally introduces a coarse-graining defect fraction of $\delta = 1/k = 1/12$. As photons traverse this late-time discrete network, the macroscopic spatial metric must kinematically stretch to absorb these unfillable structural gaps without tearing the manifold. Treating this irreducible spatial defect as a mandatory fractional volumetric extension yields the following kinematic mapping:

$$H_0^{\text{local}} = H_0^{\text{CMB}} \left(1 + \frac{1}{12} \right) = H_0^{\text{CMB}} \left(\frac{13}{12} \right). \quad (8)$$

For $H_0^{\text{CMB}} = 67.4 \text{ km s}^{-1} \text{ Mpc}^{-1}$, Equation 8 yields $H_0^{\text{local}} \simeq 73.01 \text{ km s}^{-1} \text{ Mpc}^{-1}$ (see Figure 4).

6. DISCUSSION AND FALSIFIABLE TESTS

6.1. Early-Universe Structure Formation

Because the boundary relation is operationally defined at radiative decoupling surfaces, it is not directly evaluable in the early optically thick universe. Prior to recombination ($z \gtrsim 1100$), the baryon–photon plasma was tightly coupled and photons did not define a macroscopic free-streaming boundary analogous to a photosphere. The present framework therefore does not pro-

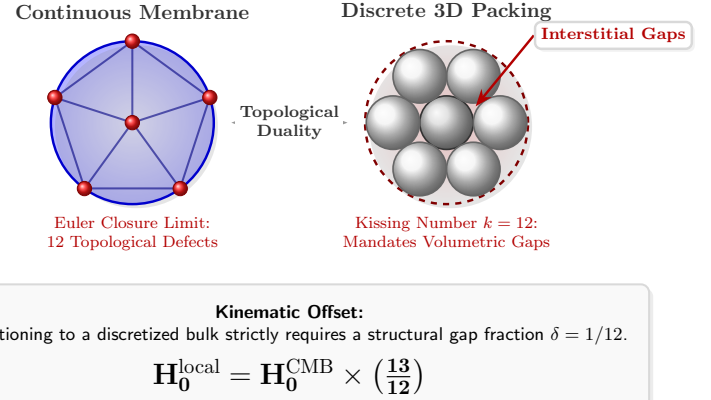


Figure 4. The topological interpretation of the H_0 offset. **Left:** A continuous spherical membrane intrinsically requires exactly 12 topological defects to close (Euler’s polyhedron theorem). **Right:** Discretizing a 3D bulk volume naturally bounds the local coordination number to $k = 12$ kissing spheres. Packing discrete spherical domains into a 3D Euclidean volume intrinsically generates interstitial empty spaces (highlighted in red). **Bottom:** Accommodating these geometric gaps forces the bulk volume to expand by a fractional extension of $1/12$, offering a geometric interpretation for the kinematic Hubble offset without parameter tuning.

vide an additional constraint on pre-recombination dynamics beyond standard gravitational instability and structure formation. No claim is made here that Λ is absent at early times; rather, this boundary normalization becomes operationally testable only once a macroscopic decoupling surface exists.

6.2. The $w = -1$ Equation of State

The observation of a dark energy equation of state $w \approx -1$ is commonly attributed to a negative-pressure dark fluid. Geometrically, however, projecting a strictly 2D surface tension (Λ) onto a 3D enclosed volume strictly requires an effective negative pressure equal in magnitude to its energy density ($P = -\rho c^2$). Thus, $w = -1$ follows as a thermodynamic identity of dimensional projection, with $P = -\rho c^2$ for a boundary tension mapped into an enclosed 3D volume. Methodologically, if the overarching macroscopic geometry natively accounts for this negative pressure, attributing this effect to an unobservable underlying dark fluid violates the Leibnizian principle of the identity of indiscernibles. Inventing hidden variables to explain what geometry already necessitates introduces unnecessary ontological baggage.

6.3. Falsifiable Tests

This framework offers several immediate avenues for empirical falsification and refinement:

1. **Expanded DEB samples:** Larger DEB compilations should sharpen the boundary relation distribution, demonstrating an even tighter convergence to $\pi^3/15 \simeq 2.0671$ as instrumental precision improves, while preserving strict mass-independence.
2. **Independent bolometric fluxes:** A stellar subsample utilizing direct bolometric flux radiometry and geometric parallax distances allows the relation to be assembled strictly without any $L \propto R^2 T_{\text{eff}}^4$ closure, isolating residual catalog circularity.
3. **Non-photospheric decoupling:** Evaluating the relation for systems with extended dynamic decoupling surfaces (e.g., strong stellar winds, Wolf-Rayet stars) will test if $\pi^3/15$ is specific to static photospheres or represents a broader radiative boundary relation.
4. **Cosmological combinations:** The precise prediction $\Omega_\Lambda = \pi^3/45$ provides a fixed target for future multi-probe constraints (CMB + BAO + Weak Lensing). The boundary-normalized target should remain stable.
5. **Fixed-factor H_0 offset:** If the topological packing mapping is correct, the empirical ratio $H_0^{\text{local}}/H_0^{\text{CMB}}$ should strictly converge to $13/12 \simeq 1.0833$ as calibrations improve, rather than drifting arbitrarily.

7. CONCLUSIONS

The framework presented proposes that macroscopic physical boundaries are governed by fundamental geometric and topological normalizations. By unpacking the algebraic anatomy of the boundary relation, this framework constrains several persistent anomalies in observational cosmology:

1. **Local Gravity Nullification:** At local decoupling surfaces (stellar photospheres), Newtonian surface gravity structurally nullifies bulk mass, revealing the 2D phase-space capacity $\pi^3/15$. This limit is verified empirically across nearly two decades of stellar mass.
2. **Global Horizon Projection:** Scaling this precise 2D capacity to the cosmic horizon via a holographic ansatz explicitly dictates the boundary tension Λ . Mapping this 2D surface capacity into a 3D bulk Friedmann density inherently yields the empirical dark energy fraction $\Omega_\Lambda = \pi^3/45 \simeq 0.6890$.

3. **Horizon Thermodynamics:** Encoding the geometric boundary constraint into a minimal mini-superspace action analytically derives the Friedmann equations and demonstrates exact structural equivalence with the Bekenstein–Hawking area-entropy law ($N = A_H/l_P^2$).
4. **The Holographic Bridge:** The canonical $\sim 10^{120}$ cosmological constant discrepancy is reframed as a dimensional area-scaling artifact. It represents the exact physical scaling ratio (A_H/l_P^2) required to tile the macroscopic horizon (Λ) with microscopic Planck areas (G).
5. **Kinematic Interpretation (H_0):** Modeling the transition from a continuous early-universe primordial fluid to a late-universe discrete void network suggests a 3D coarse-graining offset (kissing number $k = 12$). This geometrically interprets the kinematic volume scaling $H_0^{\text{local}} = H_0^{\text{CMB}}(13/12) \simeq 73.01 \text{ km s}^{-1} \text{ Mpc}^{-1}$.

Ultimately, by respecting the dimensional geometry of physical boundaries, cosmological constraints natively align with local stellar measurements, uniting local Newtonian gravity (G) and macroscopic boundary tension (Λ) under one mathematical identity (see Table 1). This unifying relation demonstrates that overarching macroscopic geometric constraints, rather than microscopic reductionism, dictate the fundamental scale limits of physical systems.

Future work will focus on expanding the empirical evaluation of the boundary capacity to a wider demographic of stellar populations, including extreme metallicity environments and compact objects, to rigorously map optical depth deviations from the theoretical limit $\pi^3/15$. Theoretically, extending the Macroscopic Boundary Principle to intermediate boundaries, specifically black hole event horizons, will further test the scale-independence of this geometric normalization.

Table 1 summarizes the geometric targets alongside representative empirical values from stellar photospheres and contemporary cosmological constraints.

DATA AVAILABILITY

The input stellar parameters are taken from the public detached eclipsing-binary compilation of [Torres et al. \(2010\)](#). All derived quantities reported in this Letter follow directly from those published measurements and can be recomputed without additional proprietary data. All figures were generated natively in L^AT_EX using TikZ and PGFPlots.

Table 1. Hierarchy of Geometric Predictions vs. Representative Empirical Values

Parameter	Geometric Prediction	Empirical Value	Reference
Boundary Relation X (Stellar)	$\pi^3/15 \simeq 2.0671$	2.0600 ± 0.0027	DEBs (Torres et al. 2010)
Dark Energy Fraction Ω_Λ	$\pi^3/45 \simeq 0.6890$	0.6889	Planck Collaboration (2020)
Matter Fraction Ω_m	$1 - \pi^3/45 \simeq 0.3110$	0.3111	Planck Collaboration (2020)
Local Expansion H_0^{local} [km s $^{-1}$ Mpc $^{-1}$]	$67.4 \times (13/12) \simeq 73.01$	73.0	Local distance ladder (Riess et al. 2024)

1 The author extends special thanks to Dr. Mehmet
 2 Keçeci for his valuable feedback and mathematical verifi-
 3 cation, which contributed to the robustness of the phys-
 4 ical arguments presented in this work. We acknowledge
 5 the observational teams and public archives that enabled
 6 the benchmark comparisons referenced in the text, in-
 7 cluding the local distance-ladder determinations cited
 8 here. Zenodo is acknowledged for open-access archiving
 9 with timestamped dissemination.

REFERENCES

- Bekenstein, J. D. 1973, Phys. Rev. D, 7, 2333
 Bousso, R. 2002, Rev. Mod. Phys., 74, 825
 Conway, J. H., & Sloane, N. J. A. 2013, *Sphere Packings, Lattices and Groups* (New York: Springer)
 Eddington, A. S. 1926, *The Internal Constitution of the Stars* (Cambridge: Cambridge Univ. Press)
 Hawking, S. W. 1975, Commun. Math. Phys., 43, 199
 Planck Collaboration. 2020, A&A, 641, A6
 Riess, A. G., et al. 2024, ApJ, 977, 120
 Schwarzschild, K. 1906, Nachr. Königl. Ges. Wiss. Göttingen, Math.-Phys. Kl., 195
 Torres, G., Andersen, J., & Giménez, A. 2010, A&ARv, 18, 67